JACS Au
AN OPEN ACCESS JOURNAL OF THE AMERICAN CHEMICAL SOCIETY

pubs.acs.org/jacsau
Article

Modular Development of Enzyme-Activatable Proteolysis Targeting Chimeras for Selective Protein Degradation and Cancer Targeting

Yanchi Chen,[‖] Lina Zhang,[‖] Lincheng Fang,[‖] Chengjie Chen, Dong Zhang, and Tao Peng*

Cite This: JACS Au 2024, 4, 2564−2577
Read Online

ACCESS | Metrics & More | Article Recommendations | Supporting Information

ABSTRACT: As an emerging therapeutic modality, proteolysis targeting chimeras (PROTACs) indiscriminately degrade proteins in both healthy and diseased cells, posing a risk of on-target off-site toxicity in normal tissues. Herein, we present the modular development of enzyme-activatable PROTACs, which utilize enzyme-recognition moieties to block protein degradation activities and can be specifically activated by elevated enzymes in cancer cells to enable cell-selective protein degradation and cancer targeting. We identified the methylene alkoxy carbamate (MAC) unit as an optimal self-immolative linker, possessing high stability and release efficiency for conjugating enzyme-recognition moieties with PROTACs. Leveraging the MAC linker, we developed a series of enzyme-activatable PROTACs, harnessing distinct enzymes for cancer-cell-selective protein degradation. Significantly, we introduced the first dual-enzyme-activatable PROTAC that requires the presence of two cancer-associated enzymes for activation, demonstrating highly selective protein degradation in cancer cells over nonmalignant cells, potent *in vivo* antitumor efficacy, and no off-tumor toxicity to normal tissues. The broad applicability of enzyme-activatable PROTACs was further demonstrated by caging other PROTACs via the MAC linker to target different proteins and E3 ligases. Our work underscores the substantial potential of enzyme-activatable PROTACs in overcoming the off-site toxicity associated with conventional PROTACs and offers new opportunities for targeted cancer treatment.

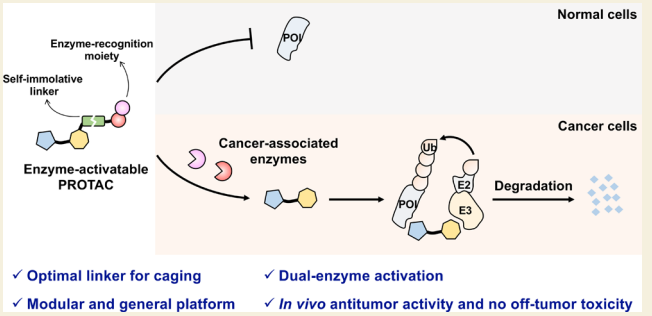

KEYWORDS: *PROTAC, enzyme-activatable, selective protein degradation, methylene alkoxy carbamate, self-immolative linker, cancer targeting*

INTRODUCTION

Proteolysis targeting chimeras (PROTACs) have emerged as a promising therapeutic modality to degrade target proteins.[1] PROTACs consist of two ligands connected by a linker, allowing them to simultaneously bind with a target protein of interest (POI) and an E3 ubiquitin ligase, such as von Hippel−Lindau (VHL) and cereblon (CRBN), to form a ternary complex that induces ubiquitination and subsequent degradation of the POI by the ubiquitin-proteasome system.[2] PROTACs offer many advantages, including the catalytic-type mechanism, event-driven pharmacology, and potential to tackle historically challenging protein targets,[3] and have garnered significant interest in both academia and industry, with numerous candidates entering clinical trials for cancer treatment.[4]

Despite these advancements, conventional PROTACs are limited by the risk of on-target off-site toxicity in normal tissues,[2b,4,5] due to lack of tumor specificity and indiscriminate degradation of essential proteins in both healthy and diseased cells. To overcome this limitation, various approaches have been proposed to enhance the targetability of conventional PROTACs,[6] including intracellularly generated PROTACs,[7] receptor-directed PROTACs,[8] and stimuli-activatable PROTACs.[9] Among them, activatable PROTACs have been highly appreciated for their ability to control protein degradation selectively in diseased cells in response to external or endogenous stimulation conditions, including light,[10] X-ray,[11] bio-orthogonal reaction,[12] reactive oxygen species,[13] and tumor microenvironment,[14] while staying inert in healthy cells.

During our efforts in harnessing the chemical and enzymatic reactivities of biomolecules to activate fluorescent probes,[15] we are particularly interested in enzyme-activatable PROTACs, especially considering that enzymes with high expression levels in cancer cells are widely recognized as promising cancer biomarkers.[16] In principle, conventional PROTACs can be caged by enzyme-recognition moieties to block their protein degradation capabilities, and elevated enzymes in cancer cells

Received: April 3, 2024
Revised: May 10, 2024
Accepted: May 10, 2024
Published: May 16, 2024

https://doi.org/10.1021/jacsau.4c00298
JACS Au 2024, 4, 2564−2577

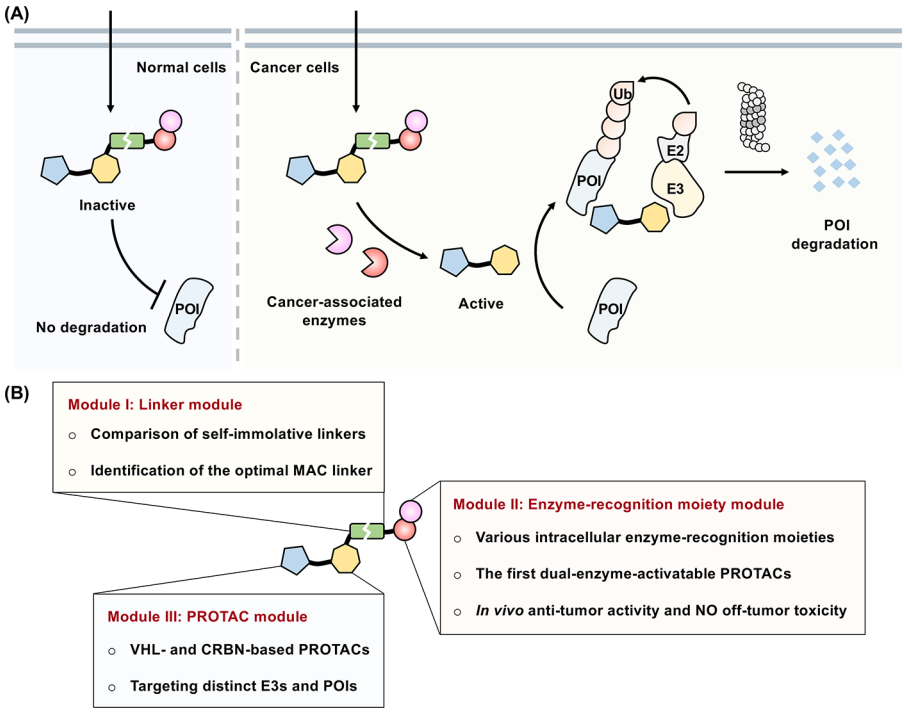

Figure 1. Enzyme-activatable PROTACs for selective protein degradation. (A) Schematic of enzyme-activatable PROTACs for selective protein degradation in cancer cells. (B) This work systematically explores the three modules of enzyme-activatable PROTACs.

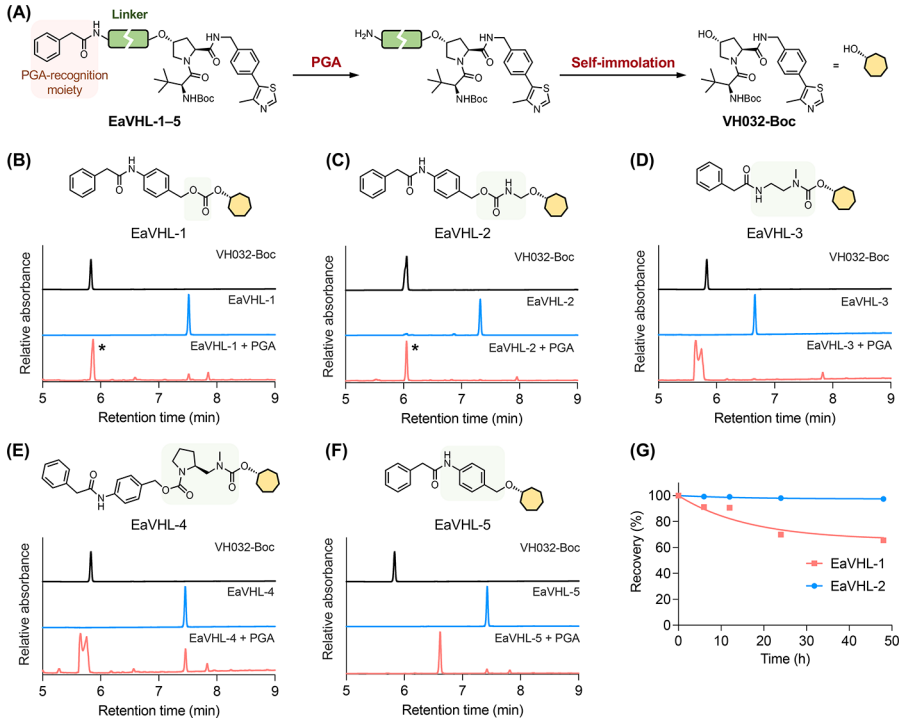

Figure 2. Comparison of self-immolative linkers for caging the VHL ligand. (A) Design of PGA-activatable VHL ligands and their activation by PGA through removal of the PGA-recognition moiety and self-immolation of the linkers. HPLC analyses on the reactions of (B) EaVHL-1, (C) EaVHL-2, (D) EaVHL-3, (E) EaVHL-4, and (F) EaVHL-5, with PGA. Asterisks in panels (B) and (C) indicate peaks of the generated VH032-Boc. (G) Stability of EaVHL-1 and EaVHL-2 in cell culture media containing 10% serum at 37 °C.

can remove these moieties, releasing active PROTACs and enabling selective degradation of POIs in cancer cells, but not in healthy cells (Figure 1A). However, the rational development of enzyme-activatable PROTACs is challenging, and a modular construction platform that is generalizable to various enzymes and PROTACs remains to be established. Additionally, while the VHL ligand of PROTACs represents a promising hotspot to install caging groups, the most commonly used linker to connect them with the VHL ligand, that is, the carbonate unit,[6,9] was found to be labile under physiological

https://doi.org/10.1021/jacsau.4c00298
JACS Au 2024, 4, 2564−2577

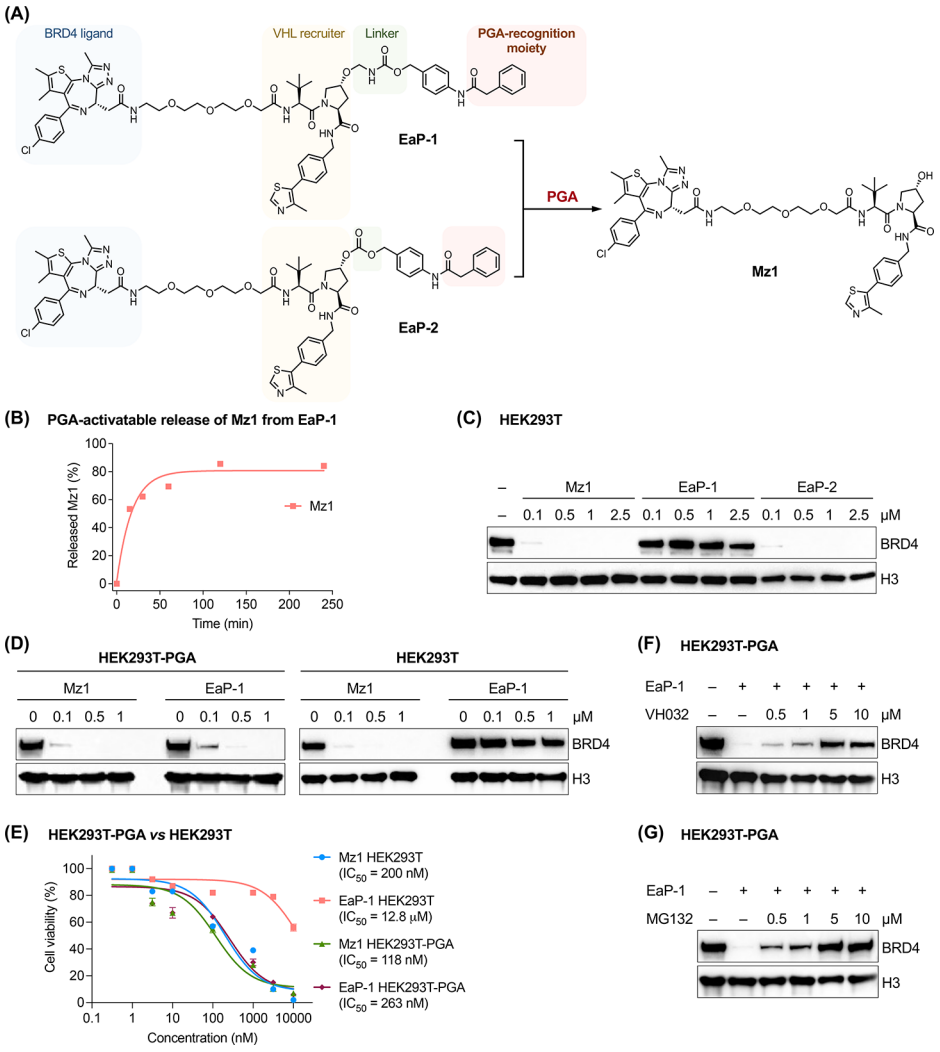

Figure 3. PGA-activatable EaP-1 enables cell-selective degradation of BRD4. (A) Structures of PGA-activatable EaP-1 and EaP-2 and the activation by PGA to generate Mz1. (B) Efficiency of PGA-activatable release of Mz1 from EaP-1 analyzed by HPLC. (C) Western blot analysis of BRD4 levels in HEK293T cells treated with indicated doses of Mz1, EaP-1, or EaP-2 for 24 h. (D) Western blot analysis of BRD4 levels in HEK293T-PGA and HEK293T cells treated with indicated doses of Mz1 or EaP-1 for 24 h. (E) Cell viability of HEK293T−PGA and HEK293T cells after treatment with Mz1 or EaP−1 for 72 h. (F) Western blot analysis of BRD4 levels in HEK293T−PGA cells after cotreated with EaP−1 (1 μM) and indicated doses of VH032 for 24 h. (G) Western blot analysis of BRD4 levels in HEK293T-PGA cells after cotreated with EaP-1 (1 μM) and indicated doses of MG132 for 24 h.

conditions,[17] probably leading to nonspecific decaging. Given that the linker structure significantly affects the stability and activation specificity of enzyme-activatable PROTACs, an optimal linker for conjugating PROTACs with enzyme-recognition moieties is desperately needed. Moreover, intracellular enzymes that are preferable to extracellular enzymes in minimizing the diffusion of activated PROTACs into nearby healthy cells are still limited for this purpose.[18] Most importantly, enzyme-activatable PROTACs that rely on a single upregulated enzyme in cancer cells may be associated with unsatisfactory cell selectivity due to the potential for false positive activation in healthy cells.[19] Dual-enzyme-activatable PROTACs, which require two cancer-associated enzymes with an additional activation criterion, offer more accurate discrimination of cancer cells from normal cells. Nevertheless, dual-enzyme-activatable PROTACs have not been reported yet.

Herein, we systematically explore the modular development of enzyme-activatable PROTACs for cell-selective protein degradation and cancer targeting. Enzyme-activatable PROTACs involve three modules (Figure 1B): the PROTAC module, which recruits the VHL or CRBN ligase and POI, the enzyme-recognition moiety module, which blocks the activity of the PROTAC and enables recognition and cleavage by the target enzyme to trigger the decaging process, and the linker module, which connects the above two modules and undergoes self-immolation after removal of the enzyme-recognition moiety to liberate the PROTAC. Through a comprehensive investigation of these modules (Figure 1B), we revealed the optimality of the methylene alkoxy carbamate (MAC) unit with high stability and release efficiency for caging conventional PROTACs, developed a range of enzyme-activatable RPOTACs, including the first dual-enzyme-activatable PROTAC that exhibits selective protein degradation in malignant cancer cells and potent *in vivo* antitumor activity without causing off-tumor toxicity, and demonstrated the wide applicability to distinct VHL- and CRBN-based PROTACs. Our findings significantly enhance the repertoire of activatable

https://doi.org/10.1021/jacsau.4c00298
JACS Au 2024, 4, 2564−2577

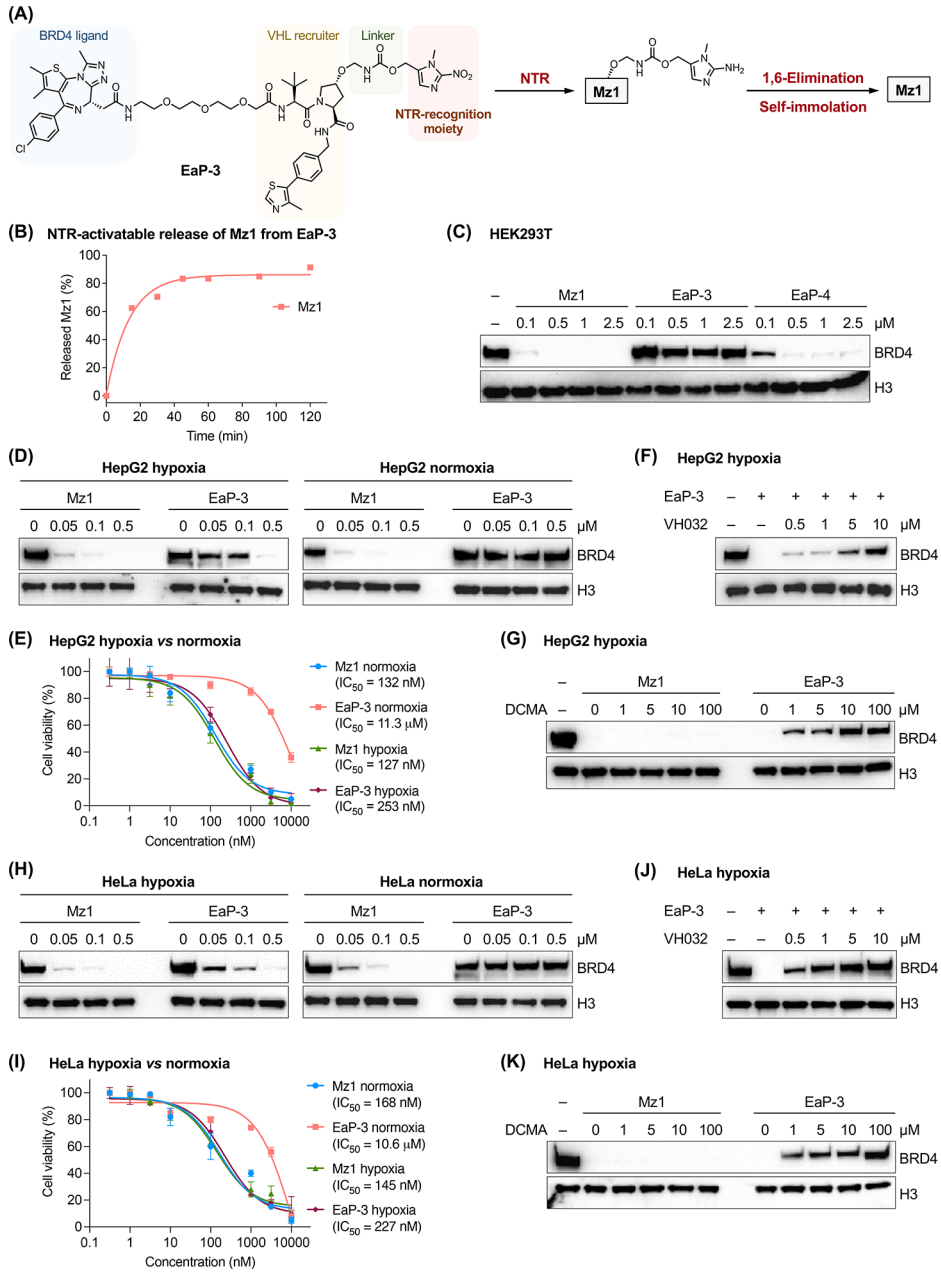

Figure 4. NTR-activatable EaP-3 enables selective degradation of BRD4 in cancer cells in an NTR-dependent manner. (A) Structure of NTR-activatable EaP-3 and the activation by NTR to generate Mz1. (B) The efficiency of NTR-activatable release of Mz1 from EaP-3 analyzed by HPLC. (C) Western blot analysis of BRD4 levels in HEK293T cells treated with indicated doses of Mz1, EaP-3, or EaP-4 for 24 h. (D, H) Western blot analysis of BRD4 levels in hypoxic and normoxic (D) HepG2 and (H) HeLa cells treated with indicated doses of Mz1 or EaP-3 for 24 h. (E, I) Cell viability of hypoxic and normoxic (E) HepG2 and (I) HeLa cells after treatment with Mz1 or EaP-3 for 72 h. (F, J) Western blot analysis of BRD4 levels in hypoxic (F) HepG2 and (J) HeLa cells after cotreated with EaP-3 (0.5 μM) and indicated doses of VH032 for 24 h. (G, K) Western blot analysis of BRD4 levels in hypoxic (G) HepG2 and (K) HeLa cells after cotreated with Mz1 or EaP-3 (0.5 μM) and indicated doses of NTR inhibitor DCMA for 24 h.

PROTACs and facilitate their applications in precise protein degradation and targeted cancer therapy.

RESULTS AND DISCUSSION

Investigation of the Linker Module for Caging the VHL Ligand

Studies have shown that the addition of a bulky group at the hydroxyl group of the VHL ligand disrupts its binding with the VHL ligase,[10e,20] which has led to the extensive development of caged PROTACs.[6,9] However, the carbonate unit almost exclusively used for connecting the VHL ligand with cages was susceptible to hydrolysis under physiological conditions,[17a] especially in the presence of ubiquitous esterases and abundant biothiols,[17b] increasing the risk of unintended release of active PROTACs in the absence of triggers. We therefore sought to find a more stable and efficient alternative for caging the VHL ligand. We chose penicillin G acylase (PGA)[21] of *Escherichia coli* origin as the model enzyme for its enzymatic activity in hydrolyzing the phenylacetyl group of its substrate phenylacetamide.[22] A series of PGA-activatable VHL ligands, EaVHL-1−5 (Figure 2 and Schemes S1−S6), were designed and

https://doi.org/10.1021/jacsau.4c00298
JACS Au 2024, 4, 2564−2577

synthesized by incorporating the phenylacetamide moiety at the hydroxyl group of the VHL ligand VH032-Boc via different self-immolative linkers,[23] including carbonate,[23] MAC,[24] ethylenediamine-carbamate,[25] proline-derived carbamate,[26] and *para*-aminobenzyl (PAB).[27] It is expected that cleavage of the phenylacetyl group by PGA generates an amine to trigger the spontaneous and sequential self-immolation processes (Figures S1−S5), such as CO_2 formation (for carbonate), hemiaminal hydrolysis (for MAC), cyclization (for ethylenediamine-carbamate and proline-derived carbamate), and 1,6-elimination (for PAB), to liberate VH032-Boc (Figure 2A). To assess the efficiency of PGA-induced VH032-Boc release, EaVHL-1−5 were incubated with PGA in an aqueous buffer and analyzed by high-performance liquid chromatography−mass spectrometry (HPLC-MS). The results showed that EaVHL-1 bearing the carbonate unit was converted into VH032-Boc in a high yield (Figures 2B and S1), and that EaVHL-2 containing the MAC linker quantitatively generated VH032-Boc upon incubation with PGA (Figures 2C and S2). By contrast, although the phenylacetyl group in EaVHL-3 and EaVHL-4 was removed by PGA and the subsequent 1,6-elimination of the PAB linker occurred smoothly, the resulting products were trapped in the amine intermediates without generation of VH032-Boc (Figures 2D,E, S3, and S4), suggesting sluggish self-immolation of the corresponding linkers. EaVHL-5 exhibited a fast decaging by PGA but an inefficient 1,6-elimination of the PAB linker, yielding a trapped aniline intermediate without VH032-Boc detected (Figures 2F and S5). We then examined the stability of EaVHL-1 and EaVHL-2. The results showed that EaVHL-2 can be quantitatively recovered upon incubation in cell culture media containing 10% serum at 37 °C, whereas EaVHL-1 decomposed slowly (Figures 2G and S6). Therefore, these data indicate that the MAC linker is highly efficient in the release of the VHL ligand and more stable than the most commonly used carbonate unit under physiological conditions.

Development of PGA-Activatable PROTAC for Cell-Selective BRD4 Degradation

The self-immolative MAC linker has so far not been used to cage VHL-based PROTACs. To confirm the utility of this linker, we designed and synthesized a PGA-activatable PROTAC, named EaP-1 (Figure 3A and Scheme S7), by installing the PGA-recognition moiety via the MAC linker onto the VHL ligand of a prototypic PROTAC Mz1,[28] the degrader of a potential cancer therapeutic target bromodomain-containing protein 4 (BRD4).[29] In vitro HPLC-MS analyses confirmed the excellent stability of EaP-1 in serum-containing culture media (Figure S7), high efficiency of PGA-triggered Mz1 release (>80% yield) (Figures 3B, S8, and S9), and fast Mz1 release kinetics with 12 min to reach half of the maximal yield (Figure 3B).

We then evaluated the capability of EaP-1 for cell-selective BRD4 degradation. In HEK293T cells lacking PGA expression, EaP-1 failed to induce BRD4 degradation (Figure 3C) as expected. Interestingly, the analogous molecule, that is, EaP-2 (Figure 3A and Scheme S7), which was similarly caged via the most commonly used carbonate unit, reduced BRD4 levels in HEK293T cells in an efficiency similar to Mz1 (Figure 3C), indicating PGA-independent nonspecific activation of EaP-2 probably due to its limited cellular stability. In contrast, in HEK293T cells stably expressing PGA (i.e., HEK293T-PGA) (Figure S10A), EaP-1 exhibited a similar efficiency to Mz1 in degrading BRD4 (Figure 3D) and a comparable cytotoxicity (Figure 3E). While Mz1 strongly inhibited the growth of HEK293T cells (IC_{50} = 200 nM), EaP-1 was found to be much less cytotoxic in HEK293T cells (IC_{50} = 12.8 μM) (Figure 3E), in line with the Western blotting results (Figure 3C,D). Using the free VHL ligand VH032,[30] the Cullin neddylation inhibitor MLN4924, and the proteasome inhibitor MG132, we confirmed that EaP-1-induced BRD4 degradation in HEK293T-PGA cells is dependent on VHL, ubiquitination, and proteasome (Figures 3F−G and S11A,B). The free PGA recognition moiety was incapable of suppressing the degradation of BRD4 (Figure S11C), which can be explained by its role as an active substrate of PGA, rather than a direct inhibitor. Overall, these results demonstrate that enzyme-activatable EaP-1 bearing the MAC linker exhibits excellent stability, high decaging efficiency, and PGA-dependent BRD4 degradation capability. The MAC linker appears to outcompete the most commonly used carbonate unit to enable cell-selective protein degradation.

Development of NTR-Activatable PROTAC for Cell-Selective BRD4 Degradation

To develop activatable PROTACs that can be specifically switched on by cancer-associated enzymes, we turned our attention to nitroreductase (NTR), an enzyme effective at catalyzing the reduction of nitroaryl groups to amines.[31] The expression level and enzymatic activity of NTR are elevated in tumor cells under hypoxia,[32] which is a pathological hallmark of solid tumors and closely related to tumor progression.[33] Our previous studies identified 2-nitro-*N*-methyl-imidazolyl as a highly efficient nitroaryl group for NTR recognition and reduction.[15c] We thus conjugated 2-nitro-*N*-methyl-imidazolyl to the hydroxyl group of the VHL ligand in Mz1 through the MAC linker, generating an NTR-activatable PROTAC, that is, EaP-3 (Scheme S8), that could be converted into Mz1 by NTR (Figure 4A). In vitro HPLC-MS analyses showed that EaP-3 was very stable in serum-containing culture media in the absence of NTR (Figure S12). By contrast, EaP-4, the analogous compound that was similarly caged via the carbonate unit (Scheme S9), was less stable and slowly decomposed to generate Mz1 under the same conditions (Figure S12). We further confirmed that incubation of EaP-3 with NTR efficiently generated Mz1 (Figure S13), the yield of which was estimated to be 62% after 15 min and reached 91% after 2 h (Figures 4B and S14).

To examine whether EaP-3 could allow selective BRD4 degradation in NTR-expressing cells, we generated HEK293T cells stably expressing NTR (i.e., HEK293T-NTR) (Figure S10B). Compared to HEK293T-NTR cells, the wild-type HEK293T cells exhibited negligible NTR activity no matter under hypoxic or normoxic conditions (Figure S10C) and were thus used as a control. Importantly, EaP-3 was unable to induce the degradation of BRD4 in wild-type HEK293T cells lacking NTR activity (Figure 4C). However, the carbonate counterpart EaP-4 was found to be almost as active as Mz1 in HEK293T cells (Figure 4C), suggesting that EaP-4 was nonspecifically activated in the absence of NTR. These results are notably consistent with those shown above for EaP-2 (Figure 3C) and again indicate that the carbonate unit is less tolerant to cellular contexts. By contrast, in HEK293T-NTR cells, EaP-3 efficiently induced BRD4 degradation and cell death in NTR-, VHL-, and proteasome-dependent manners

https://doi.org/10.1021/jacsau.4c00298
JACS Au 2024, 4, 2564−2577

(Figure S15), verifying the potential of EaP-3 to degrade BRD4 selectively in NTR-expressing cells.

We next investigated the potential of EaP-3 for selective degradation of BRD4 in cancerous HepG2 and HeLa cells that were validated to have elevated NTR activities during hypoxia (Figure S16A).[15c,32b] We found that EaP-3 dose-dependently induced BRD4 degradation in both HepG2 and HeLa cells only under hypoxic conditions but not under normoxic conditions (Figure 4D,H). The efficacy of EaP-3 in degrading BRD4 in wild-type HEK293T and cancerous cells (Figure 4C,D,H) was notably correlated with NTR activities in these cells (Figure S16A). In clear contrast, Mz1 was highly effective in degrading BRD4 in HepG2 and HeLa cells, no matter under hypoxic or normoxic conditions (Figure 4D,H). Consistent with these results, cytotoxicity assays showed that EaP-3 was comparably toxic to Mz1 in HepG2 and HeLa cells under hypoxia but was much less cytotoxic than Mz1 in these cells under normoxia (Figure 4E,I). Moreover, EaP-3 was more cytotoxic under hypoxia than under normoxia in both HepG2 (IC_{50} = 253 nM and 11.3 μM, respectively) and HeLa (IC_{50} = 227 nM and 10.6 μM, respectively) cells (Figure 4E,I), in line with its differential capabilities in inducing BRD4 degradation. Therefore, these data demonstrate the effectiveness of EaP-3 to selectively degrade BRD4 in hypoxic cancer cells. To understand the mechanism of EaP-3-induced BRD4 degradation, we demonstrated that treatment of hypoxic HepG2 and HeLa cells with VH032 (Figure 4F,J) or MG132 (Figure S16B,D) alleviated EaP-3-promoted degradation of BRD4 and that VH032 increased the IC_{50} values of EaP-3 in these cells (Figure S16C,E). More importantly, the NTR inhibitor dicoumarin (DCMA)[15c] attenuated the ability of EaP-3, but not that of Mz1, to degrade BRD4 in hypoxic HepG2 and HeLa cells (Figure 4G,K). Collectively, these results suggest that EaP-3 can be activated by endogenous NTR to enable selective BRD4 degradation in hypoxic cancer cells.

NTR-Activatable EaP-3 Inhibits *In Vivo* Tumor Growth

Given the excellent cellular activity of EaP-3, we sought to evaluate its antitumor activity *in vivo* with a mouse tumor xenograft model. The HepG2 tumor-bearing mice were generated via subcutaneous implantation of HepG2 cells. EaP-3 or Mz1 was administered at the onset of palpable tumors (~90 mm^3) through subcutaneous injection. Both the volume and weight of tumors were significantly reduced in EaP-3-treated mice compared to those in vehicle-treated mice (Figure 5A–C), suggesting that EaP-3 was activated *in vivo* to remit tumor growth with a similar efficiency to Mz1. Importantly, treatment of EaP-3 did not result in a significant loss of body weight (Figure 5D). The histopathologic analysis also demonstrated that the administration of EaP-3 exhibited little damage to major organs such as the heart, liver, spleen, lung, and kidney (Figure 5E), indicating that the observed tumor shrinkage was not due to systemic *in vivo* toxicity of EaP-3. These results demonstrate that the NTR-activatable EaP-3 efficiently suppresses the growth of HepG2 xenograft tumors *in vivo* without severe systemic toxicity.

Development of Dual-Enzyme-Activatable PROTAC for Selective BRD4 Degradation in Cancer Cells

To further enhance the activation specificity, we continued to explore dual-enzyme-activatable PROTACs that are expected to have even lower off-tumor activation owing to the requirement of successive processing by two cancer-associated enzymes. For this, we chose cancer-associated histone

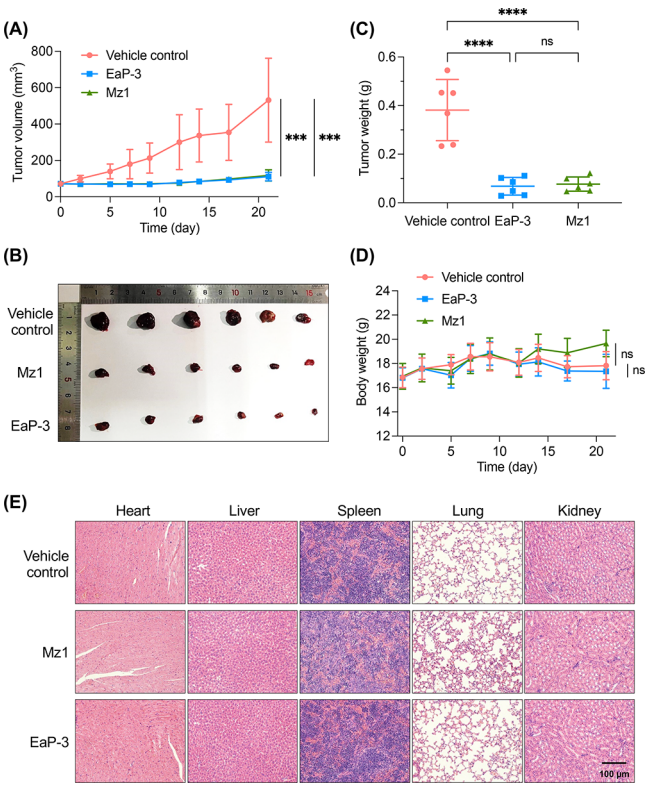

Figure 5. NTR-activatable EaP-3 inhibits tumor growth *in vivo*. (A) Tumor growth in HepG2 xenograft mice. Mice-bearing HepG2 xenograft tumors were treated with vehicle control, Mz1, or EaP-3 (25 mg/kg/dose) daily via subcutaneous injection for 21 days. (B) Images and (C) weight analysis of HepG2 tumors from mice receiving vehicle control, Mz1, or EaP-3 at the end of the experiment. (D) Body weight changes of tumor-bearing mice during the treatment in panel (A). (E) H&E staining of major organs from mice receiving vehicle control, Mz1, or EaP-3 at the end of the experiment. Data shown in panels (A), (C), and (D) are mean ± sd (n = 6 mice per group). Statistical analyses were performed with one-way ANOVA, ns $p > 0.05$, *** $p < 0.001$, **** $p < 0.0001$.

deacetylases (HDACs) and cathepsin B (CTSB), both of which have been considered to be therapeutic targets for cancer treatment.[34] HDACs are key enzymes in the regulation of protein structure and function through deacetylation of lysine residues.[35] Elevated levels of HDACs are closely related to tumorigenesis, progression, and metastasis.[36] CTSB, a cysteine protease hydrolyzing intracellular proteins with broad substrate specificity, also has crucial roles in multiple stages of development and progression, including tumor growth, angiogenesis, invasion, and metastasis.[37] CTSB is frequently overexpressed in a variety of tumors, especially colorectal cancers,[34b] while the content of CTSB in normal tissues is far lower and even negligible.[38]

To develop dual-enzyme-activatable PROTACs targeting HDACs and CTSB, we proposed to incorporate ε-*N*-acetylated lysine-based substrate motifs for HDACs and CTSB[39] into the hydroxyproline group of Mz1 via the MAC linker. It was expected that HDACs could first remove the ε-*N*-acetyl group to unmask the lysine residue, which could be recognized and cleaved by CTSB[39] to initiate the sequential elimination and liberate Mz1 (Figure 6A). We synthesized a series of candidates, that is, EaP-5–9 (Scheme S10), bearing different α-amino substituents (Figure S17), and evaluated their abilities to degrade BRD4 in human colorectal carcinoma

https://doi.org/10.1021/jacsau.4c00298
JACS Au 2024, 4, 2564–2577

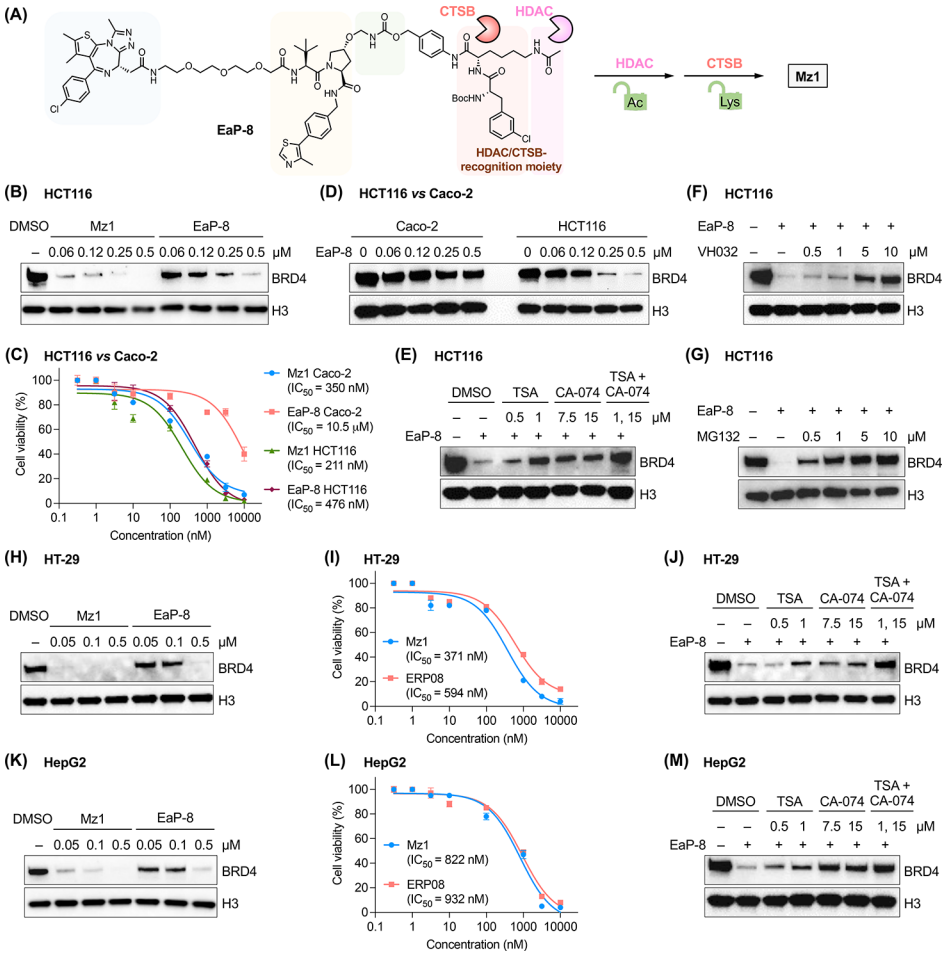

Figure 6. Dual-enzyme-activatable EaP-8 enables selective degradation of BRD4 in malignant cancer cells. (A) Structure of the dual-enzyme-activatable PROTAC EaP-8 and the activation by HDACs and CTSB to generate Mz1. (B) Western blot analysis of BRD4 levels in malignant HCT116 cells treated with indicated doses of Mz1 or EaP-8 for 24 h. (C) Cell viability of nonmalignant Caco-2 cells and malignant HCT116 cells after treatment with Mz1 or EaP-8 for 72 h. (D) Western blot analysis of BRD4 levels in nonmalignant Caco-2 cells versus malignant HCT116 cells treated with indicated doses of EaP-8 for 24 h. (E) Western blot analysis of BRD4 levels in HCT116 cells after cotreated with EaP-8 (0.5 μM) and indicated doses of HDACs inhibitor TSA, CTSB inhibitor CA-074, or both for 24 h. (F) Western blot analysis of BRD4 levels in HCT116 cells after cotreated with EaP-8 (0.5 μM) and indicated doses of VH032 for 24 h. (G) Western blot analysis of BRD4 levels in HCT116 cells after cotreated with EaP-8 (0.5 μM) and indicated doses of MG132 for 24 h. (H, K) Western blot analysis of BRD4 levels in malignant (H) HT-29 and (K) HepG2 cells treated with indicated doses of Mz1 or EaP-8 for 24 h. (I, L) Cell viability of malignant (I) HT-29 and (L) HepG2 cells after treatment with Mz1 or EaP-8 for 72 h. (J, M) Western blot analysis of BRD4 levels in (J) HT-29 and (M) HepG2 cells after cotreated with EaP-8 (0.5 μM) and indicated doses of HDACs inhibitor TSA, CTSB inhibitor CA-074, or both for 24 h.

HCT116 cells that have been reported to express high levels of HDACs and CTSB.[40] EaP-5−9 exhibited varying efficiencies in promoting BRD4 degradation that were attributed to different levels of activation and Mz1 release (Figure S17). Hydrophobic residues, such as phenylalanines in EaP-8−9 (Figure S17), substituted on the α-amino group of lysine substantially increased the efficiency in inducing BRD4 degradation. This is consistent with previous reports showing that dipeptides composed of basic and hydrophobic amino acids (e.g., the phenylalanine-lysine dipeptide) are efficient CTSB substrates.[39,41]

We focused on EaP-8 for further characterization. Western blotting and cell viability assays demonstrated comparable efficiencies of EaP-8 and Mz1 in inducing BRD4 degradation and suppressing cell growth (IC_{50} = 476 nM and 211 nM, respectively) in the malignant HCT116 cells (Figure 6B,C). To examine the selectivity of EaP-8, we used less tumorigenic colonic Caco-2 cells that are similar to normally differentiated enterocytes when cultured as confluent cells[42] and expressed basal levels of HDACs and CTSB.[40a] In nonmalignant Caco-2 cells, EaP-8 was much less efficacious in promoting BRD4 degradation than in malignant HCT116 cells (Figure 6D). Consistently, EaP-8 was much less cytotoxic in Caco-2 cells (IC_{50} = 10.5 μM) than in HCT116 cells (IC_{50} = 476 nM) (Figure 6C), whereas Mz1 was similarly cytotoxic in these two types of cells (Figure 6C). Moreover, EaP-8 was also shown to efficiently induce BRD4 degradation and inhibit cell growth in HT-29 colorectal cancer cells (Figure 6H,I) and HepG2 liver cancer cells (Figure 6K,L), both of which are malignant cancer cells having elevated activities of HDACs and CSTB as well.[40a,c,43] Therefore, these results demonstrate that EaP-8 exhibits a high degree of selectivity for malignant cancer cells with increased HDACs and CTSB activities over nonmalignant cells in mediating BRD4 degradation and cell death (Figure S18A).

To understand the mechanism and specificity of EaP-8 activation, we employed the pan-inhibitor of HDACs, that is, trichostatin A (TSA),[44] and the selective inhibitor of CTSB,

https://doi.org/10.1021/jacsau.4c00298
JACS Au 2024, 4, 2564−2577

that is, CA-074,[45] in the BRD4 degradation assay. Addition of TSA or CA-074 attenuated EaP-8-induced degradation of BRD4 in HCT116 (Figure 6E), HT-29 (Figure 6J), and HepG2 (Figure 6M) cells. The inclusion of both TSA and CA-074 even more substantially suppressed EaP-8-mediated degradation of BRD4 in these cells (Figure 6E,J,M). By contrast, EaP-8-induced BRD4 degradation was less affected by Z-FY-CHO, a specific inhibitor of CTSL,[46] compared to CA-074 and a broad-spectrum cysteine protease inhibitor E64D[47] (Figure S18B). We also showed that VH032, MG132, and MLN4924 rescued BRD4 degradation in HCT116 cells (Figures 6F,G and S18C). Similarly, VH032 and MG132 also blocked BRD4 degradation in HT-29 (Figure S18E,F) and HepG2 (Figure S18H,I) cells. In addition, VH032 attenuated the cytotoxicity of EaP-8 in these cells (Figure S18D,G,J). These results together suggest that the activities of both HDACs and CTSB are required for the activation of EaP-8, leading to BRD4 degradation and cell growth inhibition dependent on VHL and proteasome.

Dual-Activatable EaP-8 Suppresses *In Vivo* Tumor Growth without Off-Tumor Toxicity to Normal Tissues

To assess the *in vivo* antitumor efficacy of EaP-8, we used a mouse xenograft model bearing HCT116 cells. The colon cancer HCT116 cells were subcutaneously injected into the lower axilla of mice. When small palpable tumors (~90 mm^3) had developed, EaP-8 was administered subcutaneously. Mice treated with EaP-8 or Mz1 developed significantly smaller tumors in both volume and weight in comparison with vehicle-treated mice (Figure 7A–C), suggesting that EaP-8 remitted tumor growth *in vivo* as efficiently as Mz1. The administration of EaP-8 appeared to be well tolerated, as judged by body weight measurements (Figure 7D) and histopathologic staining of the major organs (Figure 7E).

A highly attractive advantage of enzyme-activatable PROTACs is the targeted activation inside tumors leading to minimal toxicity to normal tissues. We thus assessed the off-tumor toxicity of the dual-activatable EaP-8. BRD4 depletion in the skin was shown to cause epithelial hyperplasia, along with follicular dysplasia and subsequent alopecia.[48] We indeed observed obvious epithelial hyperplasia and overall deterioration of skin health near the injection sites in mice receiving Mz-1 (Figure 7F,G). In comparison, no such side effects, that is, increases in epidermal thickness, in skin tissues were observed in mice receiving EaP-8 and vehicle control (Figure 7F,G). Consistently, the immunohistochemical analysis showed a significant reduction of BRD4 in skin sections from Mz1-treated mice (Figure 7H,I), accounting for the observed phenotype of hyperplasia in the epidermis,[48a] whereas no significant BRD4 reduction was found in skin sections from EaP-8- and vehicle-treated mice (Figure 7H,I). Therefore, these results clearly demonstrate that the dual-enzyme-activatable EaP-8 exhibits potent *in vivo* antitumor efficacy and excellent tumor-specific targeting, and, most importantly, substantially ameliorates the off-tumor toxicity to healthy tissues after systemic administration.

Expansion of Dual-Enzyme-Activatable PROTAC for Selective MEK1/2 Degradation in Cancer Cells

To further examine whether enzyme-activatable PROTACs could be expanded to target other POIs, we chose MS432, a VHL-based PROTAC for degrading cancer therapeutical targets mitogen-activated protein kinase 1 and 2 (MEK1 and MEK2, i.e., MAP2K1 and MAP2K2).[49] Specifically, we

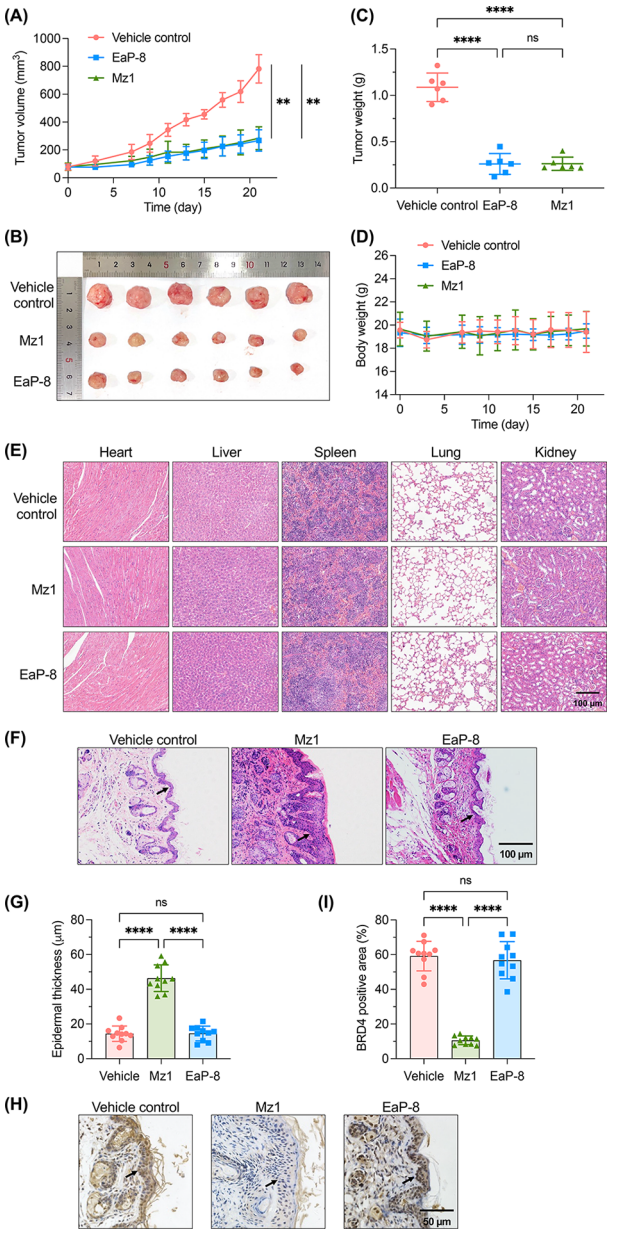

Figure 7. Dual-enzyme-activatable EaP-8 exhibits *in vivo* antitumor activity without off-tumor cytotoxicity. (A) Tumor growth in HCT116 xenograft mice. Mice-bearing HCT116 xenograft tumors were treated with vehicle control, Mz1, or EaP-8 (30 mg/kg/dose) daily via subcutaneous injection for 21 days. (B) Images and (C) weight analysis of HCT116 tumors from mice receiving vehicle control, Mz1, or EaP-8 at the end of the experiment. (D) Body weight changes of tumor-bearing mice during the treatment in panel (A). (E) H&E staining of major organs from mice receiving vehicle control, Mz1, or EaP-8 at the end of the experiment. (F) Representative H&E staining of skin sections from mice receiving vehicle control, Mz1, or EaP-8, showing epithelial hyperplasia. (G) Epidermal thickness measured in skin sections shown in panel (F). (H) Immunohistochemical analysis of BRD4 expression shown as brown signals in skin sections from mice receiving vehicle control, Mz1, or EaP-8. (I) Quantification of BRD4 positive areas in skin sections shown in panel (H). Data shown in panels (A), (C), and (D) are mean ± sd (n = 6 mice per group). Data shown in panels (G) and (I) are mean ± sd (n = 10 regions of interest from at least three samples per group). Statistical analyses were performed with one-way ANOVA, ns $p > 0.05$, ** $p < 0.01$, **** $p < 0.0001$.

https://doi.org/10.1021/jacsau.4c00298
JACS Au 2024, 4, 2564–2577

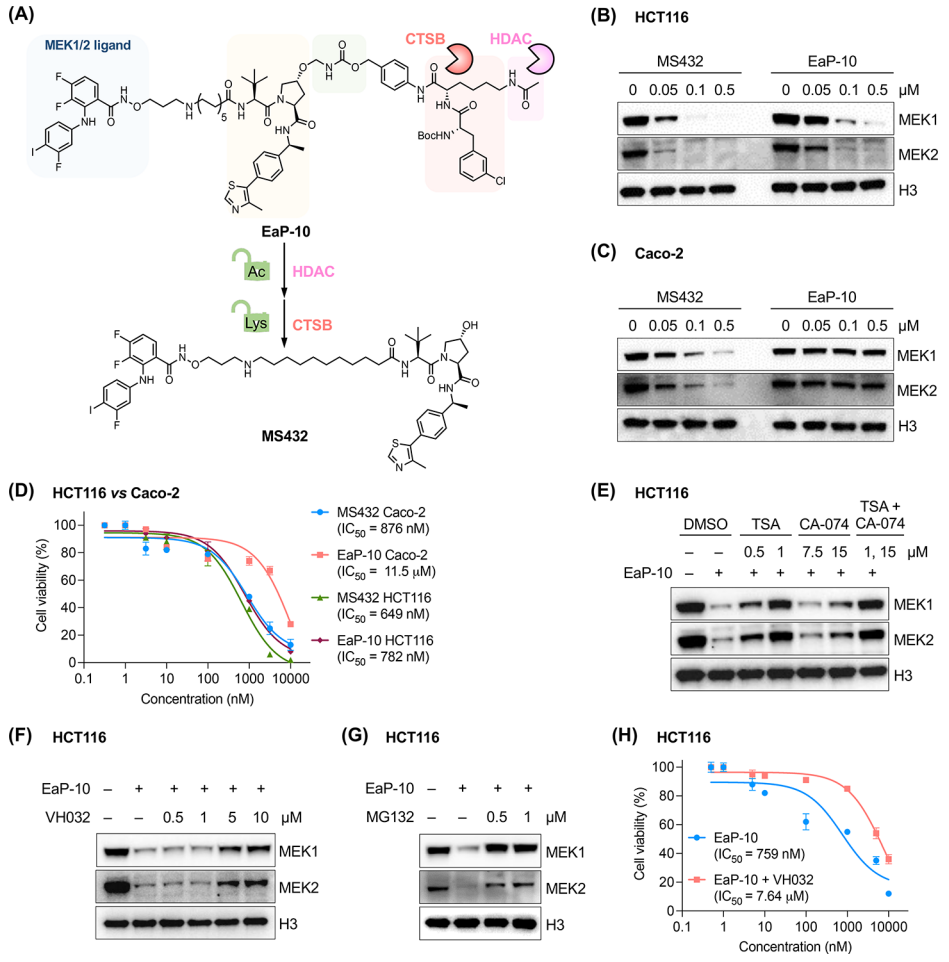

Figure 8. Dual-enzyme-activatable EaP-10 enables selective degradation of MEK1/2 in malignant cancer cells. (A) Structure of the dual-enzyme-activatable PROTAC EaP-10 and the activation by HDACs and CTSB to generate MS432. (B) Western blot analysis of MEK1/2 levels in malignant HCT116 cells treated with indicated doses of MS432 or EaP-10 for 24 h. (C) Western blot analysis of MEK1/2 levels in nonmalignant Caco-2 cells treated with indicated doses of MS432 or EaP-10 for 24 h. (D) Cell viability of nonmalignant Caco-2 cells and malignant HCT116 cells after treatment with MS432 or EaP-10 for 72 h. (E) Western blot analysis of MEK1/2 levels in HCT116 cells after cotreated with EaP-10 (0.5 μM) and indicated doses of HDACs inhibitor TSA, CTSB inhibitor CA-074, or both for 24 h. (F) Western blot analysis of MEK1/2 levels in HCT116 cells after cotreated with EaP-10 (0.5 μM) and indicated doses of free VHL ligand VH032 for 24 h. (G) Western blot analysis of MEK1/2 levels in HCT116 cells after cotreated with EaP-10 (0.5 μM) and indicated doses of MG132 for 24 h. (H) Cell viability of HCT116 cells after treatment with EaP-10 in the absence or presence of VH032 (10 μM) for 72 h.

synthesized an MS432-derived activatable PROTAC, that is, EaP-10 (Schemes S11 and 12), by caging the VHL ligand with the ε-*N*-acetylated lysine-phenylalanine substrate moiety for HDACs and CTSB via the MAC linker (Figure 8A). As expected, EaP-10 induced the degradation of MEK1/2 in malignant HCT116 cells (Figure 8B) and inhibited cell proliferation as efficiently as the parent molecule MS432 (Figure 8D). EaP-10 failed to degrade MEK1/2 in nonmalignant Caco-2 cells (Figure 8C) and exhibited a much weaker cytotoxicity than MS432 (Figure 8D). Inhibitors of HDACs and CTSB, that is, TSA and CA-074, respectively, alleviated EaP-10-mediated degradation of MEK1/2 in HCT116 cells (Figure 8E). In addition, VH032 and MG132 attenuated EaP-10-induced degradation of MEK1/2 (Figure 8F,G) and VH032 mitigated its cytotoxicity in HCT116 cells (Figure 8H). Therefore, these results suggest that EaP-10 is capable of degrading MEK1/2 selectively in malignant cancer cells in HDACs/CTSB-, VHL-, and proteasome-dependent manners.

Expansion of Enzyme-Activatable PROTACs to the CRBN Ligand

While the above enzyme-activatable PROTACs are derived from VHL-based PROTACs, we envisioned that the self-immolative MAC linker could also be applied to cage the CRBN ligand that represents another one of the two most widely used ligands in conventional PROTACs. It is worth noting that the incorporation of caging groups at the glutarimide nitrogen of thalidomide and analogues has been elusive due to unexpected issues in synthesis, release, and stability.[6a,10a,13a,50] To extend the scope of enzyme-activatable PROTACs to CRBN-based degraders, we selected a BRD4 degrader SJ995973 that comprises JQ1 and a novel CRBN binder, that is, phenyl glutarimide (PG).[50] PG analogues were recently shown to exhibit retained affinity for CRBN, improved chemical stability, and synthetic feasibility compared with classical thalidomide analogous ligands.[50] However, the application of PG in activatable PROTACs has by far not been explored. We thus designed and synthesized an NTR-activatable PROTAC, EaP-11, by incorporating 2-nitro-*N*-

https://doi.org/10.1021/jacsau.4c00298
JACS Au 2024, 4, 2564−2577

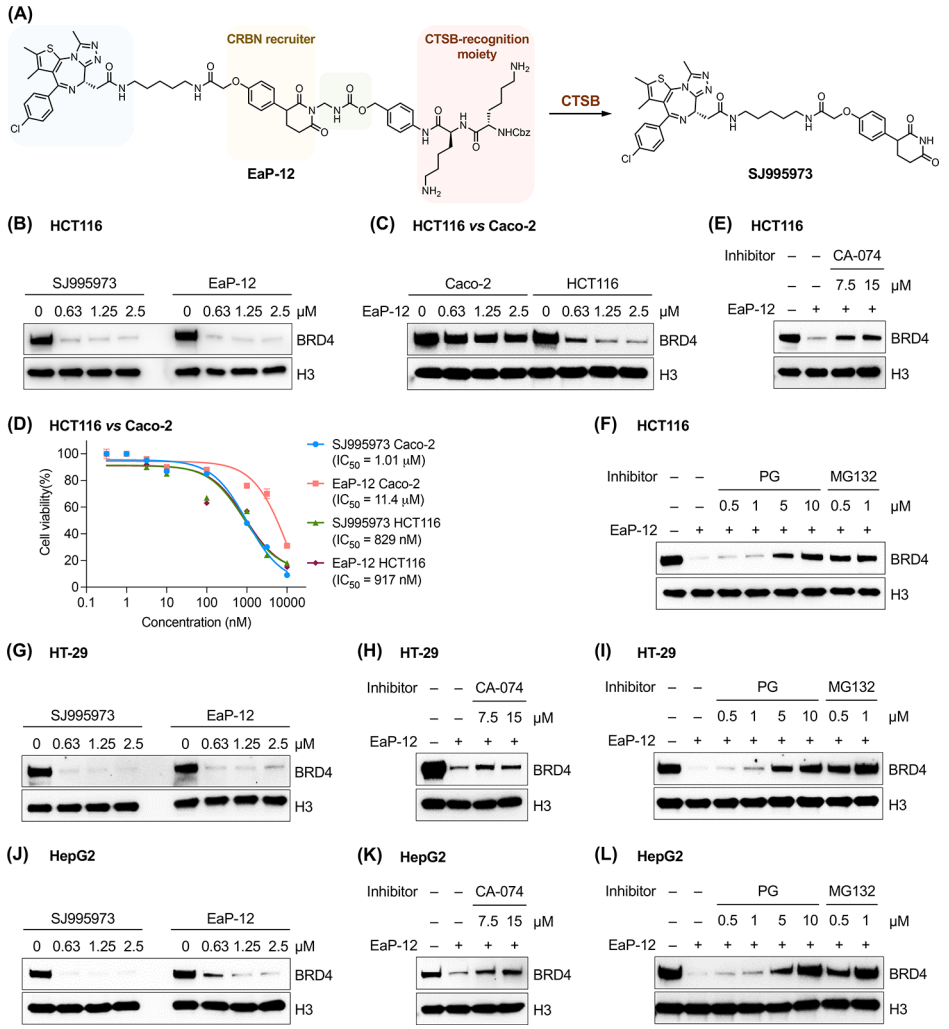

Figure 9. CTSB-activatable EaP-12 enables selective degradation of BRD4 in cancer cells in CTSB- and CRBN-dependent manners. (A) Structure of the CTSB-activatable PROTAC EaP-12 and the activation by CTSB to generate SJ995973. (B) Western blot analysis of BRD4 levels in malignant HCT116 cells treated with indicated doses of SJ995973 or EaP-12 for 24 h. (C) Western blot analysis of BRD4 levels in nonmalignant Caco-2 cells versus malignant HCT116 cells treated with indicated doses of EaP-12 for 24 h. (D) Cell viability of nonmalignant Caco-2 cells and malignant HCT116 cells after treatment with SJ995973 or EaP-12 for 72 h. (E) Western blot analysis of BRD4 levels in HCT116 cells after cotreated with EaP-12 (0.5 μM) and indicated doses of CTSB inhibitor CA-074 for 24 h. (F) Western blot analysis of BRD4 levels in HCT116 cells after cotreated with EaP-12 (0.5 μM) and indicated doses of free CRBN ligand PG or MG132 for 24 h. (G, J) Western blot analysis of BRD4 levels in malignant (G) HT-29 and (J) HepG2 cells treated with indicated doses of SJ995973 or EaP-12 for 24 h. (H, K) Western blot analysis of BRD4 levels in (H) HT-29 and (K) HepG2 cells after cotreated with EaP-12 (0.5 μM) and indicated doses of CTSB inhibitor CA-074 for 24 h. (I, L) Western blot analysis of BRD4 levels in (I) HT-29 and (L) HepG2 cells after cotreated with EaP-12 (0.5 μM) and indicated doses of free CRBN ligand PG or MG132 for 24 h.

methyl-imidazolyl at the imide moiety of PG in SJ995973 via the MAC linker (Figure S19A and Schemes S13−14). Western blotting analysis showed that EaP-11 induced BRD4 degradation in HEK293T-NTR and hypoxic HepG2 cells, but not in wild-type HEK293T and normoxic HepG2 cells (Figure S19B−E). Therefore, these data suggest that *N*-alkylation at the imide moiety blocks the binding of PG to CRBN, as for thalidomide.[51]

To demonstrate the broad applicability, we synthesized a CTSB-activatable PROTAC, that is, EaP-12 (Scheme S15), by incorporating a highly specific CTSB-recognition lysine−lysine dipeptide substrate[52] into the PG moiety of SJ995973 via the MAC linker (Figure 9A). EaP-12, like SJ995973, efficiently degraded BRD4 in malignant HCT116 cells (Figure 9B). Importantly, EaP-12 degraded BRD4 more efficiently in HCT116 cells than in nonmalignant Caco-2 cells (Figure 9C). Consistently, cell viability assay indicated similar cytotoxicity of EaP-12 and SJ995973 in HCT116 cells (Figure 9D). The IC_{50} value of EaP-12 was however much higher than that of SJ99597312 in Caco-2 cells (Figure 9D). Moreover, the specific CTSB inhibitor CA-074 antagonized the effect of EaP-12 on BRD4 degradation (Figure 9E), confirming the critical role of CTSB in activating EaP-12. PG, the free CRBN ligand, and MG132 inhibited EaP-12-induced BRD4 degradation in HCT116 cells (Figure 9F), and that PG significantly increased the IC_{50} of EaP-12 (Figure S20A), suggesting that EaP-12 degraded BRD4 in CRBN- and proteasome-dependent manners. Moreover, EaP-12 also efficiently degraded BRD4 (Figure 9G,J) and exhibited comparable cytotoxicity to SJ995973 (Figure S20B,D) in malignant HT-29 and HepG2 cells, which was dependent on the CTSB activity, CRBN, and proteasome (Figures 9H,I,K,L and S20C,E). Overall, these

https://doi.org/10.1021/jacsau.4c00298
JACS Au 2024, 4, 2564−2577

results demonstrate that EaP-11 and EaP-12 can differentiate malignant cancer cells from nonmalignant cells to enable selective BRD4 degradation and that the self-immolative MAC linker and enzyme-recognition moieties can be applied to cage the PG ligand for developing enzyme-activatable CRBN-based PROTACs.

CONCLUSIONS

In conclusion, we report a systematic investigation of the modular construction of enzyme-activatable PROTACs for cancer cell-selective protein degradation and precise cancer targeting. Our findings highlight the superiority of the MAC structure as a linker for caging the VHL ligand, compared to the most commonly used carbonate unit that was shown to be less stable and intolerant to cellular contexts. Using the MAC linker, we developed a set of enzyme-activatable VHL-based PROTACs with different enzyme-recognition moieties, enabling selective protein degradation in cells expressing distinct intracellular enzymes. Most importantly, we for the first time introduced dual-enzyme-activatable PROTACs that are double-locked and operate in an AND logic manner to enhance specificity for discriminating tumor cells from normal cells. We experimentally validated that the dual-enzyme-activatable BRD4 degrader EaP-8 significantly ameliorates the *in vivo* off-tumor toxicity associated with the conventional parent PROTAC. To the best of our knowledge, this is the first direct experimental evidence to demonstrate the much improved off-tumor toxicity of activatable PROTACs. Moreover, by enclosing other conventional PROTACs, we demonstrated that the MAC linker can be applied to the CRBN recruiter and constructed additional enzyme-activatable PROTACs for targeting different proteins through alternative E3 ligases. Overall, our work thoroughly demonstrates the modularity, general applicability, and versatility of the chimeric enzyme-activatable PROTACs, addresses the off-tumor toxicity concern of conventional PROTACs, and holds great promise for PROTAC-based drug development and targeted therapy.

ASSOCIATED CONTENT

Supporting Information

The Supporting Information is available free of charge at https://pubs.acs.org/doi/10.1021/jacsau.4c00298.

Supplementary Figures S1−20, experimental procedures including chemical synthesis and biological assays, and characterization of all new compounds (PDF)

AUTHOR INFORMATION

Corresponding Author

Tao Peng − *State Key Laboratory of Chemical Oncogenomics, School of Chemical Biology and Biotechnology, Peking University Shenzhen Graduate School, Shenzhen 518055, China; Institute of Chemical Biology, Shenzhen Bay Laboratory, Shenzhen 518132, China;* orcid.org/0000-0002-5578-5314; Email: tpeng@pku.edu.cn

Authors

Yanchi Chen − *State Key Laboratory of Chemical Oncogenomics, School of Chemical Biology and Biotechnology, Peking University Shenzhen Graduate School, Shenzhen 518055, China; National Key Laboratory of Non-Food Biomass Energy Technology, National Engineering Research Center for Non-Food Biorefinery, Institute of Grand Health, Guangxi Academy of Sciences, Nanning 530007, China*

Lina Zhang − *State Key Laboratory of Chemical Oncogenomics, School of Chemical Biology and Biotechnology, Peking University Shenzhen Graduate School, Shenzhen 518055, China*

Lincheng Fang − *State Key Laboratory of Chemical Oncogenomics, School of Chemical Biology and Biotechnology, Peking University Shenzhen Graduate School, Shenzhen 518055, China*

Chengjie Chen − *State Key Laboratory of Chemical Oncogenomics, School of Chemical Biology and Biotechnology, Peking University Shenzhen Graduate School, Shenzhen 518055, China*

Dong Zhang − *State Key Laboratory of Chemical Oncogenomics, School of Chemical Biology and Biotechnology, Peking University Shenzhen Graduate School, Shenzhen 518055, China*

Complete contact information is available at: https://pubs.acs.org/10.1021/jacsau.4c00298

Author Contributions

[‖]Y.C., L.Z., and L.F. contributed equally. The manuscript was written through contributions of all authors. All authors have given approval to the final version of the manuscript. CRediT: **Yanchi Chen** investigation, methodology, resources, writing-original draft; **Lina Zhang** data curation, investigation, methodology, writing-original draft, writing-review & editing; **Lincheng Fang** investigation, resources, writing-original draft, writing-review & editing; **Chengjie Chen** investigation, resources; **Dong Zhang** investigation, resources; **Tao Peng** conceptualization, funding acquisition, project administration, supervision, writing-original draft, writing-review & editing.

Notes

The authors declare no competing financial interest.

ACKNOWLEDGMENTS

This study was approved by the Institutional Animal Care and Use Committee of Peking University Shenzhen Graduate School. We thank the Laboratory Animal Center at Peking University Shenzhen Graduate School for animal experiments. T.P. acknowledges grant support from National Natural Science Foundation of China (22277008), Shenzhen Science and Technology Innovation Committee (GXWD20201231165807007-20200814103057002), and Shenzhen-Hong Kong Institute of Brain Science-Shenzhen Fundamental Research Institutions (2023SHIBS0004).

REFERENCES

(1) (a) Sakamoto, K. M.; Kim, K. B.; Kumagai, A.; Mercurio, F.; Crews, C. M.; Deshaies, R. J. Protacs: Chimeric molecules that target proteins to the Skp1−Cullin−F box complex for ubiquitination and degradation. *Proc. Natl. Acad. Sci. U.S.A.* **2001**, *98*, 8554−8559. (b) Lai, A. C.; Crews, C. M. Induced protein degradation: an emerging drug discovery paradigm. *Nat. Rev. Drug Discovery* **2017**, *16*, 101−114.

(2) (a) Pettersson, M.; Crews, C. M. PROteolysis TArgeting Chimeras (PROTACs) — Past, present and future. *Drug Discovery Today: Technologies* **2019**, *31*, 15−27. (b) Békés, M.; Langley, D. R.; Crews, C. M. PROTAC targeted protein degraders: the past is prologue. *Nat. Rev. Drug Discovery* **2022**, *21*, 181−200.

(3) Li, K.; Crews, C. M. PROTACs: past, present and future. *Chem. Soc. Rev.* **2022**, *51*, 5214−5236.
(4) Chirnomas, D.; Hornberger, K. R.; Crews, C. M. Protein degraders enter the clinic — a new approach to cancer therapy. *Nat. Rev. Clin. Oncol.* **2023**, *20*, 265−278.
(5) (a) Khan, S.; He, Y.; Zhang, X.; Yuan, Y.; Pu, S.; Kong, Q.; Zheng, G.; Zhou, D. PROteolysis TArgeting Chimeras (PROTACs) as emerging anticancer therapeutics. *Oncogene* **2020**, *39*, 4909−4924. (b) Dale, B.; Cheng, M.; Park, K.-S.; Kaniskan, H. Ü.; Xiong, Y.; Jin, J. Advancing targeted protein degradation for cancer therapy. *Nat. Rev. Cancer* **2021**, *21*, 638−654.
(6) (a) Chen, C.; Yang, Y.; Wang, Z.; Li, H.; Dong, C.; Zhang, X. Recent Advances in Pro-PROTAC Development to Address On-Target Off-Tumor Toxicity. *J. Med. Chem.* **2023**, *66*, 8428−8440. (b) Yao, R.; Luo, T.; Wang, M. Delivering on Cell-Selective Protein Degradation Using Chemically Tailored PROTACs. *ChemBioChem.* **2023**, *24*, No. e202300413.
(7) (a) Lebraud, H.; Wright, D. J.; Johnson, C. N.; Heightman, T. D. Protein Degradation by In-Cell Self-Assembly of Proteolysis Targeting Chimeras. *ACS Cent. Sci.* **2016**, *2*, 927−934. (b) Do, T. C.; Lau, J. W.; Sun, C.; Liu, S.; Kha, K. T.; Lim, S. T.; Oon, Y. Y.; Kwan, Y. P.; Ma, J. J.; Mu, Y.; Liu, X.; Carney, T. J.; Wang, X.; Xing, B. Hypoxia deactivates epigenetic feedbacks via enzyme-derived clicking proteolysis-targeting chimeras. *Sci. Adv.* **2022**, *8*, No. eabq2216.
(8) (a) Pillow, T. H.; Adhikari, P.; Blake, R. A.; Chen, J.; Del Rosario, G.; Deshmukh, G.; Figueroa, I.; Gascoigne, K. E.; Kamath, A. V.; Kaufman, S.; Kleinheinz, T.; Kozak, K. R.; Latifi, B.; Leipold, D. D.; Sing Li, C.; Li, R.; Mulvihill, M. M.; O'Donohue, A.; Rowntree, R. K.; Sadowsky, J. D.; Wai, J.; Wang, X.; Wu, C.; Xu, Z.; Yao, H.; Yu, S.-F.; Zhang, D.; Zang, R.; Zhang, H.; Zhou, H.; Zhu, X.; Dragovich, P. S. Antibody Conjugation of a Chimeric BET Degrader Enables *in vivo* Activity. *ChemMedChem.* **2020**, *15*, 17−25. (b) Maneiro, M.; Forte, N.; Shchepinova, M. M.; Kounde, C. S.; Chudasama, V.; Baker, J. R.; Tate, E. W. Antibody−PROTAC Conjugates Enable HER2-Dependent Targeted Protein Degradation of BRD4. *ACS Chem. Biol.* **2020**, *15*, 1306−1312. (c) Liu, J.; Chen, H.; Liu, Y.; Shen, Y.; Meng, F.; Kaniskan, H. Ü.; Jin, J.; Wei, W. Cancer Selective Target Degradation by Folate-Caged PROTACs. *J. Am. Chem. Soc.* **2021**, *143*, 7380−7387. (d) He, S.; Gao, F.; Ma, J.; Ma, H.; Dong, G.; Sheng, C. Aptamer-PROTAC Conjugates (APCs) for Tumor-Specific Targeting in Breast Cancer. *Angew. Chem., Int. Ed.* **2021**, *60*, 23299−23305. (e) Chen, H.; Liu, J.; Kaniskan, H. Ü.; Wei, W.; Jin, J. Folate-Guided Protein Degradation by Immunomodulatory Imide Drug-Based Molecular Glues and Proteolysis Targeting Chimeras. *J. Med. Chem.* **2021**, *64*, 12273−12285. (f) Song, C.; Jiao, Z.; Hou, Z.; Wang, R.; Lian, C.; Xing, Y.; Luo, Q.; An, Y.; Yang, F.; Wang, Y.; Sha, X.; Ruan, Z.; Ye, Y.; Liu, Z.; Li, Z.; Yin, F. Selective Protein of Interest Degradation through the Split-and-Mix Liposome Proteolysis Targeting Chimera Approach. *J. Am. Chem. Soc.* **2023**, *145*, 21860−21870.
(9) Gao, J.; Yang, L.; Lei, S.; Zhou, F.; Nie, H.; Peng, B.; Xu, T.; Chen, X.; Yang, X.; Sheng, C.; Rao, Y.; Pu, K.; Jin, J.; Xu, Z.; Yu, H. Stimuli-activatable PROTACs for precise protein degradation and cancer therapy. *Sci. Bull.* **2023**, *68*, 1069−1085.
(10) (a) Xue, G.; Wang, K.; Zhou, D.; Zhong, H.; Pan, Z. Light-Induced Protein Degradation with Photocaged PROTACs. *J. Am. Chem. Soc.* **2019**, *141*, 18370−18374. (b) Pfaff, P.; Samarasinghe, K. T. G.; Crews, C. M.; Carreira, E. M. Reversible Spatiotemporal Control of Induced Protein Degradation by Bistable Photo-PROTACs. *ACS Cent. Sci.* **2019**, *5*, 1682−1690. (c) Kounde, C. S.; Shchepinova, M. M.; Saunders, C. N.; Muelbaier, M.; Rackham, M. D.; Harling, J. D.; Tate, E. W. A caged E3 ligase ligand for PROTAC-mediated protein degradation with light. *Chem. Commun.* **2020**, *56*, 5532−5535. (d) Liu, J.; Chen, H.; Ma, L.; He, Z.; Wang, D.; Liu, Y.; Lin, Q.; Zhang, T.; Gray, N.; Kaniskan, H. Ü.; Jin, J.; Wei, W. Light-induced control of protein destruction by opto-PROTAC. *Sci. Adv.* **2020**, *6*, No. eaay5154. (e) Naro, Y.; Darrah, K.; Deiters, A. Optical Control of Small Molecule-Induced Protein Degradation. *J. Am. Chem. Soc.* **2020**, *142*, 2193−2197. (f) Reynders, M.; Trauner, D. Optical control of targeted protein degradation. *Cell Chem. Biol.* **2021**, *28*, 969−986.
(11) Yang, C.; Yang, Y.; Li, Y.; Ni, Q.; Li, J. Radiotherapy-Triggered Proteolysis Targeting Chimera Prodrug Activation in Tumors. *J. Am. Chem. Soc.* **2023**, *145*, 385−391.
(12) Chang, M.; Gao, F.; Pontigon, D.; Gnawali, G.; Xu, H.; Wang, W. Bioorthogonal PROTAC Prodrugs Enabled by On-Target Activation. *J. Am. Chem. Soc.* **2023**, *145*, 14155−14163.
(13) (a) Liu, H.; Ren, C.; Sun, R.; Wang, H.; Zhan, Y.; Yang, X.; Jiang, B.; Chen, H. Reactive oxygen species-responsive Pre-PROTAC for tumor-specific protein degradation. *Chem. Commun.* **2022**, *58*, 10072−10075. (b) Yu, D.; Fan, H.; Zhou, Z.; Zhang, Y.; Sun, J.; Wang, L.; Jia, Y.; Tian, J.; Campbell, A.; Mi, W.; Sun, H. Hydrogen Peroxide-Inducible PROTACs for Targeted Protein Degradation in Cancer Cells. *ChemBioChem.* **2023**, *24*, No. e202300422.
(14) (a) Cheng, W.; Li, S.; Wen, X.; Han, S.; Wang, S.; Wei, H.; Song, Z.; Wang, Y.; Tian, X.; Zhang, X. Development of hypoxia-activated PROTAC exerting a more potent effect in tumor hypoxia than in normoxia. *Chem. Commun.* **2021**, *57*, 12852−12855. (b) An, K.; Deng, X.; Chi, H.; Zhang, Y.; Li, Y.; Cheng, M.; Ni, Z.; Yang, Z.; Wang, C.; Chen, J.; Bai, J.; Ran, C.; Wei, Y.; Li, J.; Zhang, P.; Xu, F.; Tan, W. Stimuli-Responsive PROTACs for Controlled Protein Degradation. *Angew. Chem., Int. Ed.* **2023**, *62*, No. e202306824.
(15) (a) Zhang, Y.; Du, Y.; Li, M.; Zhang, D.; Xiang, Z.; Peng, T. Activity-Based Genetically Encoded Fluorescent and Luminescent Probes for Detecting Formaldehyde in Living Cells. *Angew. Chem., Int. Ed.* **2020**, *59*, 16352−16356. (b) Du, Y.; Zhang, Y.; Huang, M.; Wang, S.; Wang, J.; Liao, K.; Wu, X.; Zhou, Q.; Zhang, X.; Wu, Y.-D.; Peng, T. Systematic investigation of the aza-Cope reaction for fluorescence imaging of formaldehyde *in vitro* and *in vivo*. *Chem. Sci.* **2021**, *12*, 13857−13869. (c) Wang, S.; Wu, X.; Zhang, Y.; Zhang, D.; Xie, B.; Pan, Z.; Ouyang, K.; Peng, T. Discovery of a highly efficient nitroaryl group for detection of nitroreductase and imaging of hypoxic tumor cells. *Org. Biomol. Chem.* **2021**, *19*, 3469−3478.
(16) (a) Kobayashi, H.; Ogawa, M.; Alford, R.; Choyke, P. L.; Urano, Y. New Strategies for Fluorescent Probe Design in Medical Diagnostic Imaging. *Chem. Rev.* **2010**, *110*, 2620−2640. (b) Kumar, R. R.; Kumar, A.; Chuang, C.-H.; Shaikh, M. O. Recent Advances and Emerging Trends in Cancer Biomarker Detection Technologies. *Ind. Eng. Chem. Res.* **2023**, *62*, 5691−5713.
(17) (a) Govindan, S. V.; Cardillo, T. M.; Sharkey, R. M.; Tat, F.; Gold, D. V.; Goldenberg, D. M. Milatuzumab−SN-38 Conjugates for the Treatment of CD74+ Cancers. *Mol. Cancer Ther.* **2013**, *12*, 968−978. (b) Rautio, J.; Meanwell, N. A.; Di, L.; Hageman, M. J. The expanding role of prodrugs in contemporary drug design and development. *Nat. Rev. Drug Discovery* **2018**, *17*, 559−587.
(18) (a) Liang, C.; Zheng, Q.; Luo, T.; Cai, W.; Mao, L.; Wang, M. Enzyme-Catalyzed Activation of Pro-PROTAC for Cell-Selective Protein Degradation. *CCS Chem.* **2022**, *4*, 3809−3819. (b) Shi, S.; Du, Y.; Zou, Y.; Niu, J.; Cai, Z.; Wang, X.; Qiu, F.; Ding, Y.; Yang, G.; Wu, Y.; Xu, Y.; Zhu, Q. Rational Design for Nitroreductase (NTR)-Responsive Proteolysis Targeting Chimeras (PROTACs) Selectively Targeting Tumor Tissues. *J. Med. Chem.* **2022**, *65*, 5057−5071.
(19) Wu, L.; Huang, J.; Pu, K.; James, T. D. Dual-locked spectroscopic probes for sensing and therapy. *Nat. Rev. Chem.* **2021**, *5*, 406−421.
(20) Buckley, D. L.; Van Molle, I.; Gareiss, P. C.; Tae, H. S.; Michel, J.; Noblin, D. J.; Jorgensen, W. L.; Ciulli, A.; Crews, C. M. Targeting the von Hippel−Lindau E3 Ubiquitin Ligase Using Small Molecules To Disrupt the VHL/HIF-1α Interaction. *J. Am. Chem. Soc.* **2012**, *134*, 4465−4468.
(21) Marešová, H.; Plačková, M.; Grulich, M.; Kyslík, P. Current state and perspectives of penicillin G acylase-based biocatalyses. *Appl. Microbiol. Biotechnol.* **2014**, *98*, 2867−2879.
(22) Margolin, A. L.; Švedas, V. K.; Berezin, I. V. Substrate specificity of penicillin amidase from *E. coli*. *Biochim. Biophys. Acta, Enzymol.* **1980**, *616*, 283−289.

https://doi.org/10.1021/jacsau.4c00298
JACS Au 2024, 4, 2564−2577

(23) Alouane, A.; Labruère, R.; Le Saux, T.; Schmidt, F.; Jullien, L. Self-Immolative Spacers: Kinetic Aspects, Structure−Property Relationships, and Applications. *Angew. Chem., Int. Ed.* **2015**, *54*, 7492−7509.
(24) Madec-Lougerstay, R.; Florent, J.-C.; Monneret, C. Synthesis of self-immolative glucuronide spacers based on aminomethylcarbamate. Application to 5-fluorouracil prodrugs for antibody-directed enzyme prodrug therapy. *Journal of the Chemical Society, Perkin. Transactions* **1999**, *1*, 1369−1376.
(25) Saari, W. S.; Schwering, J. E.; Lyle, P. A.; Smith, S. J.; Engelhardt, E. L. Cyclization-activated prodrugs. Basic carbamates of 4-hydroxyanisole. *J. Med. Chem.* **1990**, *33*, 97−101.
(26) Dal Corso, A.; Borlandelli, V.; Corno, C.; Perego, P.; Belvisi, L.; Pignataro, L.; Gennari, C. Fast Cyclization of a Proline-Derived Self-Immolative Spacer Improves the Efficacy of Carbamate Prodrugs. *Angew. Chem., Int. Ed.* **2020**, *59*, 4176−4181.
(27) Carl, P. L.; Chakravarty, P. K.; Katzenellenbogen, J. A. A novel connector linkage applicable in prodrug design. *J. Med. Chem.* **1981**, *24*, 479−480.
(28) Zengerle, M.; Chan, K.-H.; Ciulli, A. Selective Small Molecule Induced Degradation of the BET Bromodomain Protein BRD4. *ACS Chem. Biol.* **2015**, *10*, 1770−1777.
(29) Lu, J.; Qian, Y.; Altieri, M.; Dong, H.; Wang, J.; Raina, K.; Hines, J.; Winkler, J. D.; Crew, A. P.; Coleman, K.; Crews, C. M. Hijacking the E3 Ubiquitin Ligase Cereblon to Efficiently Target BRD4. *Chem. Biol.* **2015**, *22*, 755−763.
(30) Galdeano, C.; Gadd, M. S.; Soares, P.; Scaffidi, S.; Van Molle, I.; Birced, I.; Hewitt, S.; Dias, D. M.; Ciulli, A. Structure-Guided Design and Optimization of Small Molecules Targeting the Protein−Protein Interaction between the von Hippel−Lindau (VHL) E3 Ubiquitin Ligase and the Hypoxia Inducible Factor (HIF) Alpha Subunit with in Vitro Nanomolar Affinities. *J. Med. Chem.* **2014**, *57*, 8657−8663.
(31) Sharma, A.; Arambula, J. F.; Koo, S.; Kumar, R.; Singh, H.; Sessler, J. L.; Kim, J. S. Hypoxia-targeted drug delivery. *Chem. Soc. Rev.* **2019**, *48*, 771−813.
(32) (a) Okuda, K.; Okabe, Y.; Kadonosono, T.; Ueno, T.; Youssif, B. G. M.; Kizaka-Kondoh, S.; Nagasawa, H. 2-Nitroimidazole-Tricarbocyanine Conjugate as a Near-Infrared Fluorescent Probe for *in Vivo* Imaging of Tumor Hypoxia. *Bioconjugate Chem.* **2012**, *23*, 324−329. (b) Li, Y.; Sun, Y.; Li, J.; Su, Q.; Yuan, W.; Dai, Y.; Han, C.; Wang, Q.; Feng, W.; Li, F. Ultrasensitive Near-Infrared Fluorescence-Enhanced Probe for *in Vivo* Nitroreductase Imaging. *J. Am. Chem. Soc.* **2015**, *137*, 6407−6416.
(33) (a) Harris, A. L. Hypoxia — a key regulatory factor in tumour growth. *Nat. Rev. Cancer* **2002**, *2*, 38−47. (b) Chen, Z.; Han, F.; Du, Y.; Shi, H.; Zhou, W. Hypoxic microenvironment in cancer: molecular mechanisms and therapeutic interventions. *Signal Transduct. Target. Ther.* **2023**, *8*, 70.
(34) (a) Minucci, S.; Pelicci, P. G. Histone deacetylase inhibitors and the promise of epigenetic (and more) treatments for cancer. *Nature Reviews Cancer* **2006**, *6*, 38−51. (b) Olson, O. C.; Joyce, J. A. Cysteine cathepsin proteases: regulators of cancer progression and therapeutic response. *Nat. Rev. Cancer* **2015**, *15*, 712−729.
(35) Falkenberg, K. J.; Johnstone, R. W. Histone deacetylases and their inhibitors in cancer, neurological diseases and immune disorders. *Nat. Rev. Drug Discovery* **2014**, *13*, 673−691.
(36) (a) Ropero, S.; Esteller, M. The role of histone deacetylases (HDACs) in human cancer. *Mol. Oncol.* **2007**, *1*, 19−25. (b) Weichert, W. HDAC expression and clinical prognosis in human malignancies. *Cancer Lett.* **2009**, *280*, 168−176.
(37) (a) Mohamed, M. M.; Sloane, B. F. multifunctional enzymes in cancer. *Nat. Rev. Cancer* **2006**, *6*, 764−775. (b) Wang, J.; Zheng, M.; Yang, X.; Zhou, X.; Zhang, S. The Role of Cathepsin B in Pathophysiologies of Non-tumor and Tumor tissues: A Systematic Review. *J. Cancer* **2023**, *14*, 2344−2358.
(38) Xing, R.; Addington, A. K.; Mason, R. W. Quantification of cathepsins B and L in cells. *Biochem. J.* **1998**, *332*, 499−505.
(39) Dubowchik, G. M.; Firestone, R. A. Cathepsin B-sensitive dipeptide prodrugs. 1. A model study of structural requirements for efficient release of doxorubicin. *Bioorg. Med. Chem. Lett.* **1998**, *8*, 3341−3346.
(40) (a) Ueki, N.; Lee, S.; Sampson, N. S.; Hayman, M. J. Selective cancer targeting with prodrugs activated by histone deacetylases and a tumour-associated protease. *Nat. Commun.* **2013**, *4*, 2735. (b) Hulkower, K. I.; Butler, C. C.; Linebaugh, B. E.; Klaus, J. L.; Keppler, D.; Giranda, V. L.; Sloane, B. F. Fluorescent microplate assay for cancer cell-associated cathepsin B. *Eur. J. Biochem.* **2000**, *267*, 4165−4170. (c) Poreba, M.; Groborz, K.; Vizovisek, M.; Maruggi, M.; Turk, D.; Turk, B.; Powis, G.; Drag, M.; Salvesen, G. S. Fluorescent probes towards selective cathepsin B detection and visualization in cancer cells and patient samples. *Chem. Sci.* **2019**, *10*, 8461−8477.
(41) (a) Dubowchik, G. M.; Mosure, K.; Knipe, J. O.; Firestone, R. A. Cathepsin B-sensitive dipeptide prodrugs. 2. Models of anticancer drugs paclitaxel (Taxol®), mitomycin C and doxorubicin. *Bioorg. Med. Chem. Lett.* **1998**, *8*, 3347−3352. (b) Dubowchik, G. M.; Firestone, R. A.; Padilla, L.; Willner, D.; Hofstead, S. J.; Mosure, K.; Knipe, J. O.; Lasch, S. J.; Trail, P. A. Cathepsin B-Labile Dipeptide Linkers for Lysosomal Release of Doxorubicin from Internalizing Immunoconjugates: Model Studies of Enzymatic Drug Release and Antigen-Specific In Vitro Anticancer Activity. *Bioconjugate Chem.* **2002**, *13*, 855−869.
(42) Mariadason, J. M.; Velcich, A.; Wilson, A. J.; Augenlicht, L. H.; Gibson, P. R. Resistance to butyrate-induced cell differentiation and apoptosis during spontaneous Caco-2 cell differentiation. *Gastroenterology* **2001**, *120*, 889−899.
(43) Cheng, X.; Li, Y.; Zhou, D.; Chen, D.; Zhao, F.; Wang, W. Identification of cathepsin B as a novel target of hypoxia-inducible factor-1-alpha in HepG2 cells. *Biochem. Biophys. Res. Commun.* **2018**, *503*, 1057−1062.
(44) Yoshida, M.; Kijima, M.; Akita, M.; Beppu, T. Potent and specific inhibition of mammalian histone deacetylase both *in vivo* and *in vitro* by trichostatin A. *J. Biol. Chem.* **1990**, *265*, 17174−17179.
(45) Montaser, M.; Lalmanach, G.; Mach, L. CA-074, But Not Its Methyl Ester CA-074Me, Is a Selective Inhibitor of Cathepsin B within Living Cells. *Biol. Chem.* **2002**, *383*, 1305−1308.
(46) Gonzalez-Suarez, I.; Redwood, A. B.; Grotsky, D. A.; Neumann, M. A.; Cheng, E. H. Y.; Stewart, C. L.; Dusso, A.; Gonzalo, S. A new pathway that regulates 53BP1 stability implicates Cathepsin L and vitamin D in DNA repair. *EMBO J.* **2011**, *30*, 3383−3396.
(47) Murray, E. J. B.; Grisanti, M. S.; Bentley, G. V.; Murray, S. S. E64d, a membrane-permeable cysteine protease inhibitor, attenuates the effects of parathyroid hormone on osteoblasts in vitro. *Metabolism* **1997**, *46*, 1090−1094.
(48) (a) Bolden, J. E.; Tasdemir, N.; Dow, L. E.; van Es, J. H.; Wilkinson, J. E.; Zhao, Z.; Clevers, H.; Lowe, S. W. Inducible *In Vivo* Silencing of Brd4 Identifies Potential Toxicities of Sustained BET Protein Inhibition. *Cell Rep.* **2014**, *8*, 1919−1929. (b) Raina, K.; Lu, J.; Qian, Y.; Altieri, M.; Gordon, D.; Rossi, A. M. K.; Wang, J.; Chen, X.; Dong, H.; Siu, K.; Winkler, J. D.; Crew, A. P.; Crews, C. M.; Coleman, K. G. PROTAC-induced BET protein degradation as a therapy for castration-resistant prostate cancer. *Proc. Natl. Acad. Sci. U.S.A.* **2016**, *113*, 7124−7129.
(49) Wei, J.; Hu, J.; Wang, L.; Xie, L.; Jin, M. S.; Chen, X.; Liu, J.; Jin, J. Discovery of a First-in-Class Mitogen-Activated Protein Kinase Kinase 1/2 Degrader. *J. Med. Chem.* **2019**, *62*, 10897−10911.
(50) Min, J.; Mayasundari, A.; Keramatnia, F.; Jonchere, B.; Yang, S. W.; Jarusiewicz, J.; Actis, M.; Das, S.; Young, B.; Slavish, J.; Yang, L.; Li, Y.; Fu, X.; Garrett, S. H.; Yun, M.-K.; Li, Z.; Nithianantham, S.; Chai, S.; Chen, T.; Shelat, A.; Lee, R. E.; Nishiguchi, G.; White, S. W.; Roussel, M. F.; Potts, P. R.; Fischer, M.; Rankovic, Z. Phenyl-Glutarimides: Alternative Cereblon Binders for the Design of PROTACs. *Angew. Chem., Int. Ed.* **2021**, *60*, 26663−26670.
(51) Buhimschi, A. D.; Armstrong, H. A.; Toure, M.; Jaime-Figueroa, S.; Chen, T. L.; Lehman, A. M.; Woyach, J. A.; Johnson, A. J.; Byrd, J. C.; Crews, C. M. Targeting the C481S Ibrutinib-Resistance

https://doi.org/10.1021/jacsau.4c00298
JACS Au 2024, 4, 2564−2577

Mutation in Bruton's Tyrosine Kinase Using PROTAC-Mediated Degradation. *Biochemistry* **2018**, *57*, 3564−3575.
(52) Chowdhury, M. A.; Moya, I. A.; Bhilocha, S.; McMillan, C. C.; Vigliarolo, B. G.; Zehbe, I.; Phenix, C. P. Prodrug-Inspired Probes Selective to Cathepsin B over Other Cysteine Cathepsins. *J. Med. Chem.* **2014**, *57*, 6092−6104.

https://doi.org/10.1021/jacsau.4c00298
JACS Au 2024, 4, 2564−2577